



## Accelerated Publication

# Characterization of ion/electron beam induced deposition of electrical contacts at the sub- $\mu\text{m}$ scale

D. Brunel<sup>a,\*</sup>, D. Troadec<sup>a</sup>, D. Hourlier<sup>a</sup>, D. Deresmes<sup>a</sup>, M. Zdrojek<sup>b</sup>, T. Mélin<sup>a</sup>

<sup>a</sup> Institut d'Electronique, de Microélectronique et de Nanotechnologie, CNRS UMR 8520, Avenue Poincaré, F-59652 Villeneuve d'Ascq, France

<sup>b</sup> Faculty of Physics, Warsaw University of Technology, Koszykowa 75, 00-662 Warsaw, Poland

## ARTICLE INFO

## Article history:

Received 31 January 2011

Accepted 9 March 2011

Available online 21 March 2011

## Keywords:

FIB

Electron beam induced deposition

Ion beam induced deposition

Transport measurements

Four probe measurements

Carbon nanotube

## ABSTRACT

We investigate the fabrication of electrical contacts using ion- and electron-beam induced deposition of platinum at the sub- $\mu\text{m}$  scale. Halos associated with the metal surface decoration are characterized electrically in the 0.05–2  $\mu\text{m}$  range using transport measurements, conducting atomic force microscopy and Kelvin probe microscopy. In contrast with IBID, EBID electrodes are shown to exhibit a low leakage resistance (above 1 M $\Omega$ ) at the sub-100 nm scale, and are thus suitable to achieve resist-free electrical contacts for transport measurements on nanostructures. Four-point transport data using  $\mu\text{m}$ -spaced EBID contacts are provided for a multiwalled carbon nanotube.

© 2011 Elsevier B.V. All rights reserved.

Low-dimensional nanostructures such as carbon nanotubes, semiconductor nanowires, or graphene nanoribbons [1–3] are promising materials for nanoelectronics applications such as electronic or biological sensors [4,5]. The most common technique to connect nanostructures is electron beam lithography (EBL) [6], which enables routine fabrication of electrical contacts with sub-100 nm gap spacing. However, EBL may suffer from two disadvantages: (i) it is a process which requires multiple technological steps; (ii) EBL resist and lift-off chemicals are not compatible with some materials such as e.g. conjugated polymer nanowires [7]. This is why direct metal deposition techniques excluding resist patterning are being developed, such as e.g. nanostencil [8], and ion-beam induced metal deposition [9], respectively based on atomic force microscopy (AFM) and focused ion beam (FIB) microscopy.

We focus here on the use of IBID or EBID techniques for metal contact patterning. They are based on a sub-100 nm local deposition of metallo-organic compounds (usually containing Pt or W) under a focused ion or electron beam. In spite of early promises as a direct-writing method [10], IBID and EBID have rapidly shown limitations, such as: a FIB-induced amorphization under IBID contacts [11]; a FIB-induced change in transport properties up to  $\sim 10 \mu\text{m}$  away from IBID contacts [9]; a larger resistivity of EBID contacts as compared to IBID [10,12]; and the formation of halos and leakage pathways around IBID and EBID contacts [10] associated with a metal decoration of the sample surface, up a  $\sim 10 \mu\text{m}$

scale [13]. These features have so far restricted the use of IBID and EBID to the fabrication of electrical contacts with minimum 5–10  $\mu\text{m}$  gap spacing [9,10].

In this Letter, we investigate the fabrication of electrical contacts using IBID and EBID techniques at the sub- $\mu\text{m}$  scale. Halos associated with metal surface decoration are characterized electrically at the sub- $\mu\text{m}$  scale (i.e. 0.05–2  $\mu\text{m}$ ), using transport measurements, conducting AFM and Kelvin probe microscopy. Our results demonstrate that EBID leakage resistances fall in the M $\Omega$  range at the sub- $\mu\text{m}$  scale, in contrast with IBID leakage resistances in the k $\Omega$  range. This demonstrates that EBID can be used for sub- $\mu\text{m}$  scale contact patterning, in conjunction with four-point transport measurements to account for the high-resistivity of EBID contact patterns. An example is provided in the case of a multiwalled carbon nanotube.

Experiments have been conducted with a FEI Strata dual-beam DB235 FIB system, enabling IBID and EBID platinum deposition from a trimethylcyclopentadienyl-platinum ( $\text{CH}_3$ )<sub>3</sub>CH<sub>3</sub>C<sub>5</sub>H<sub>4</sub>Pt metallo-organic precursor gas. To characterize IBID and EBID deposited electrodes (conductivity and leakage paths), we first used test samples, consisting in EBL pre-patterned 25 nm thick gold electrodes with 5  $\mu\text{m}$  gap spacing laying on a 200 nm thick SiO<sub>2</sub> layer thermally grown from a doped silicon substrate. Experiments on contacted carbon nanotubes have been performed using predefined EBL electrodes separated by  $\sim 10 \mu\text{m}$  on a similar substrate, and commercial multiwalled nanotubes (Nanocyl) deposited from a dispersion in dichloromethane. AFM experiments have been conducted on a Dimension/Nanoscope IV AFM (Brüker-Nano), either

\* Corresponding author.

E-mail address: [david.brunel@gmail.com](mailto:david.brunel@gmail.com) (D. Brunel).

in conducting-AFM (c-AFM) or Kelvin Force Microscopy (KFM) modes, using EFM PPP (Nanosensors) cantilevers ( $k = 1\text{--}3\text{ N/m}$ ,  $f_0 \sim 75\text{ kHz}$ ). An Agilent 4155 semiconductor parameter analyzer was used for transport measurements.

The electrical properties of the deposited Pt-based materials are first characterized by measuring the resistance of IBID (Fig. 1a and EBID (Fig. 1b bars of nominal size  $8 \times 0.5\ \mu\text{m}^2$  and  $7 \times 0.5\ \mu\text{m}^2$  between predefined EBL Au contacts. The following FIB operating conditions have been used for IBID and EBID: 10 kV (5 kV) acceleration voltage, 10 pA (0.4 nA)  $\text{Ga}^+$  (electron) beam current, 1  $\mu\text{s}$

(0.5  $\mu\text{s}$ ) dwell time, and 18 s (600 s) total exposure time. The material resistivities obtained from the bar resistance and thickness (as measured from AFM) equal respectively  $\rho_{\text{IBID}} = 4\ \mu\Omega\text{ m}$  and  $\rho_{\text{EBID}} = 0.2\ \Omega\text{ m}$ . The value for IBID falls fairly close to Pt resistivity  $\rho_{\text{Pt}} = 0.11\ \mu\Omega\text{ m}$ , while it is much higher for EBID due to a lower Pt content, in agreement with previous reports [10,12].

We now focus on the halos surrounding the deposited IBID (resp. EBID) patterns in Fig. 1a (resp. Fig. 1b). The halos have been previously attributed to metal surface decoration [13] leading to leakage pathways at the  $10\ \mu\text{m}$  scale [10], but have not been

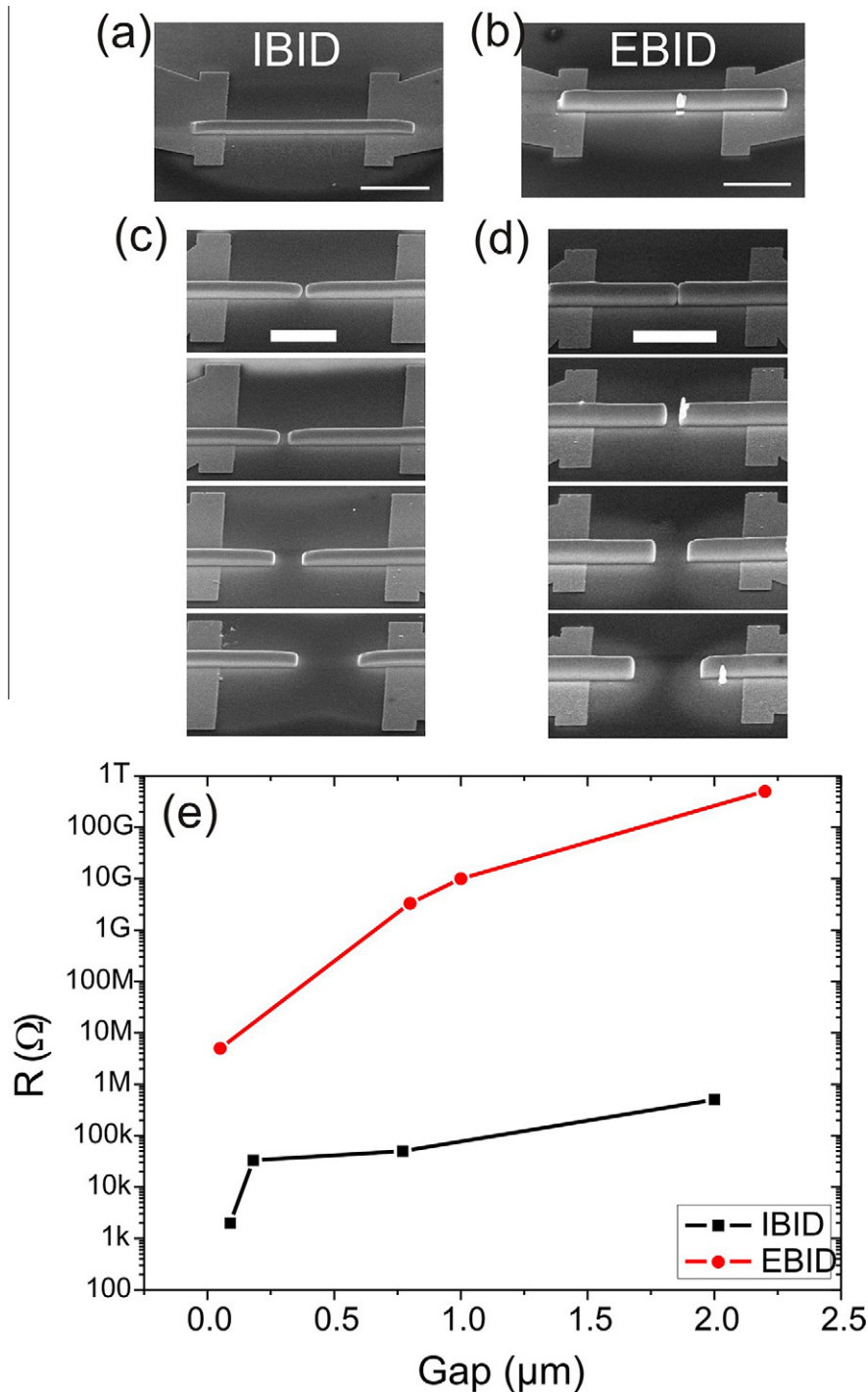


**Fig. 1.** SEM images of (a) an IBID Pt pattern and (b) an EBID Pt pattern (scale bar:  $2\ \mu\text{m}$ ). (c) Series of gaps defined by IBID from top to bottom: 0.1, 0.2, 0.8, and  $2\ \mu\text{m}$ . (d) Series of gaps defined by EBID from top to bottom: 0.05, 0.5, 1, and  $2.3\ \mu\text{m}$ . (e) Gap resistance plotted as a function of gap length.

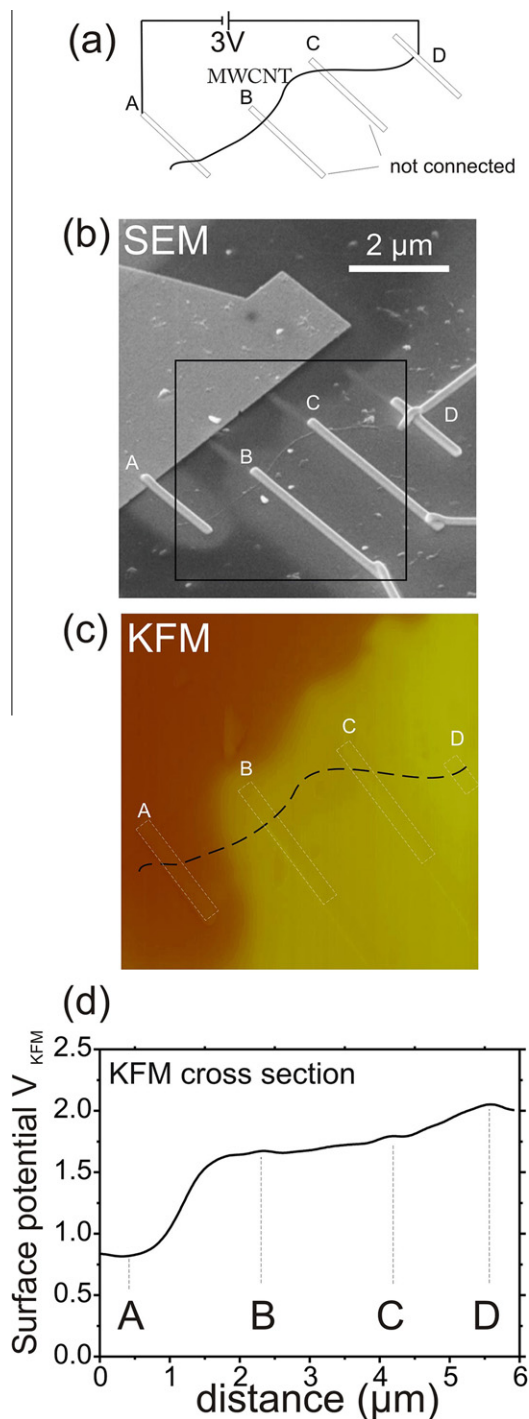


**Fig. 2.** (a) Schematics of the MWCNT contacted by four IBID electrodes. (b) SEM image of the device. (c) Corresponding KFM image. The scan frame corresponds to the black square in (b). Electrode (A) and the substrate are grounded; +3 V is applied to (D), and (B) and (C) are unconnected. (d) Surface potential cross-section taken along the dashed line in (c).

characterized so far at the sub- $\mu\text{m}$  scale. This is done in Fig. 1c (IBID) and Fig. 1d (EBID) in which series of IBID or EBID gapped electrodes have been fabricated, with a central gap of length 0.1  $\mu\text{m}$ , 0.2  $\mu\text{m}$ , 0.8  $\mu\text{m}$  and 2  $\mu\text{m}$  (IBID), and 0.05  $\mu\text{m}$ , 0.5  $\mu\text{m}$ , 1  $\mu\text{m}$  and 2.3  $\mu\text{m}$  (EBID). The gap resistance versus gap length is plotted in Fig. 1e. IBID halos are seen to be fairly conductive (a few  $\text{k}\Omega$  for gaps below 1  $\mu\text{m}$ ), and thus unsuitable to probe transport properties of nanodevices with resistance close to  $1/G_0$  [14]. In

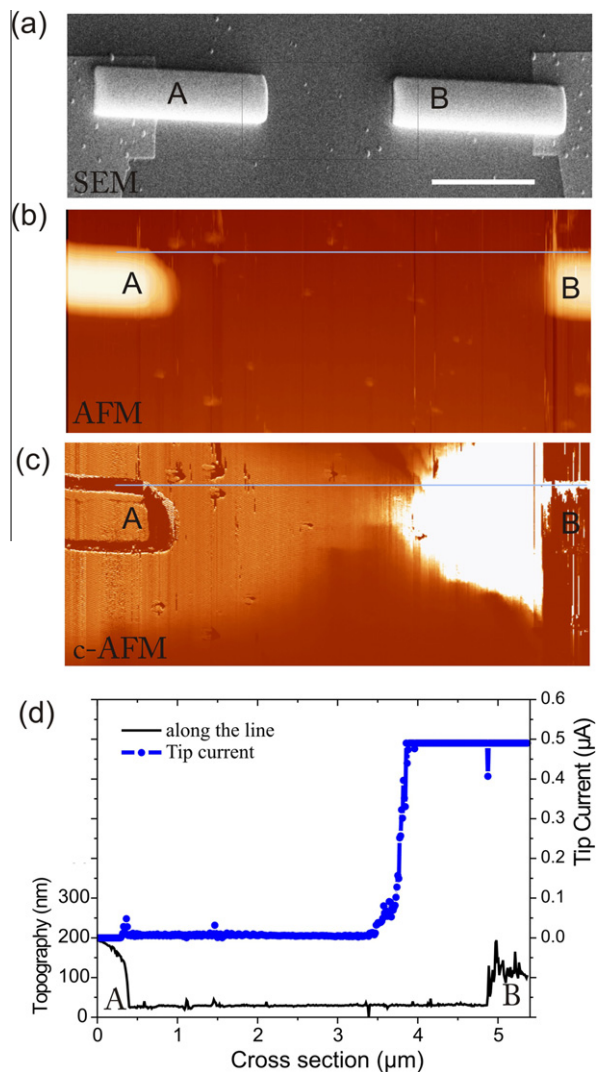


**Fig. 3.** (a) SEM image of IBID Pt patterns with a 4.5  $\mu\text{m}$  gap (scale bar: 4  $\mu\text{m}$ ) (b) AFM image and (c) conductive-AFM image of the device. The scan frame corresponds to the black square in (a). (d) Cross-section of the topography and the tip-current along the blue lines respectively in Fig. 3b and Fig. 3c.

contrast, the resistance of EBID halos is found between a few  $\text{M}\Omega$  and a few  $\text{G}\Omega$  (gaps smaller than 1  $\mu\text{m}$ ), which is consistent with nanodevice transport.

To support these conclusions, we used KFM to image the electrostatic potential distribution over a multiwalled carbon nanotube (MWCNT) connected with IBID (see Fig. 2a and SEM image in Fig. 2b). It is visible from Fig. 2b that the halos around three electrodes (B, C, and D) overlap each other, while one electrode (A) appears disconnected from its nearest neighbour (B). This is confirmed by the electrical KFM image of Fig. 2c, in which the MWCNT device is imaged with the substrate and electrode A at ground, the electrode D biased at +3 V, and the electrodes B and C unconnected. Dark contrasts in Fig. 2c correspond to surface potentials close to 0 V, and bright contrasts to positive electrostatic potentials. The three electrodes B, C, and D are almost isopotential, which is confirmed by the cross-section shown in Fig. 2d, in which the voltage drop only occurs between the electrodes with disconnected halos A and B [15]. KFM measurements thus spatially reveal that the use of IBID is limited by the presence of the parasitic halos surrounding the metal deposition [10].

The leakage issue through halos is finally further confirmed by local transport measurements. IBID electrodes with a 4.5  $\mu\text{m}$  gap

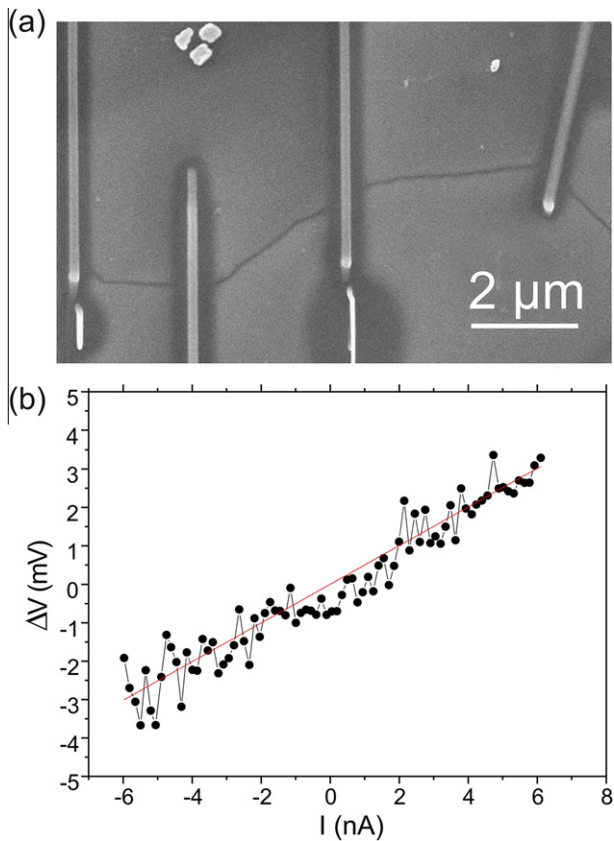


**Fig. 4.** (a) SEM image of a 10 nm diameter MWCNT contacted by four EBID electrodes (scale bar: 1  $\mu\text{m}$ ). (b) Current  $I$  flowing through the nanotube as a function of the voltage drop  $\Delta V$  measured between the two internal electrodes (device resistance: 500  $\text{k}\Omega$ ).

have been investigated using c-AFM (see Fig. 3a), in which one of the electrodes (B) is biased at +8 V while the second electrode (A) and the metallized AFM tip are left at ground. The c-AFM measurement consists in mapping the current which passes through the tip (see Fig. 3c) when scanned in contact mode over the device. Results show that the IBID halos exhibit a noticeable conduction. The local resistance through the tip is here of a few tens of  $\text{M}\Omega$  at a distance  $\sim 1 \mu\text{m}$  from the biased electrode (B). This is much lower than the leakage resistance through IBID gaps in Fig. 1 at the same distance (typically a few tens of  $\text{k}\Omega$ ), as due to the tip contact size. The leakage resistance however shows the same

exponential-like increase of typically one decade per  $\mu\text{m}$ , as in the electrical measurements of Fig. 1.

We finally illustrate the possibility to electrically characterize devices contacted by EBID at the  $\mu\text{m}$ -scale [16]. A SEM image of an EBID contacted MWCNT is shown in Fig. 4a. To circumvent the high resistance of the EBID leads, the device has been measured using a four probe measurement scheme. The  $I(\Delta V)$  characteristics is shown in Fig. 4b ( $\Delta V$  is the voltage drop between internal leads), and shows a metallic behaviour with resistance  $\sim 500 \text{k}\Omega$  consistent with MWCNTs probed with EBL contacts [17].

In conclusion, we have evaluated in this Letter the direct patterning of electrical contacts at the sub- $\mu\text{m}$  scale using IBID and EBID metal deposition in a focused ion beam microscope. IBID was found unsuitable to probe transport properties of devices at the  $\mu\text{m}$ -scale due to conductive halos around patterned electrodes, as seen from transport, c-AFM and KFM. EBID is on the other hand demonstrated as a probe of transport properties at the  $\mu\text{m}$  scale, however using four-point measurement schemes to account for the deposited electrode higher resistivity. This work has been funded in part by an ANR grant N $^{\circ}$  ANR-05-JCJC-0090. We thank C. Boyaval for technical assistance.

## References

- [1] S. Iijima, *Nature* 354 (1991) 56–58.
- [2] A.M. Morales, C.M. Lieber, *Science* 279 (1998) 208–211.
- [3] P. Avouris, Z. Chen, V. Perebeinos, *Nat. Nanotechnol.* 2 (2007) 605–615.
- [4] I. Heller, A.M. Janssens, J. Mannik, E.D. Minot, S.G. Lemay, C. Dekker, *Nano Lett.* 8 (2008) 591.
- [5] J.N. Tey, P.M. Wijaya, Z. Wang, W.H. Goh, A. Palaniappan, S. Mhaisalkar, I. Rodriguez, S. Dunham, J.A. Rogers, *Appl. Phys. Lett.* 94 (2009) 013107.
- [6] Y.Y. Wei, G. Eres, *Phys. Lett.* 76 (2000) 3759–3761.
- [7] Y.Z. Long, J.L. Duvail, M.M. Li, C. Gu, Z. Liu, S.P. Ringer, *Nanoscale Res. Lett.* 5 (2010) 237–242.
- [8] H. Guo, D. Martrou, T. Zambelli, E. Dujardin, S. Gauthier, *Rev. Sci. Instrum.* 79 (2008) 103904.
- [9] G. Chen, E.M. Gallo, J. Burger, B. Nabet, A. Cola, P. Prete, N. Lovergine, J.E. Spanier, *Appl. Phys. Lett.* 96 (2010) 223107.
- [10] V. Gopal, V.R. Radmilovic, C. Daraio, S. Jin, E.A. Yang, *Stach Nano Lett.* 4 (2004) 2059–2063.
- [11] C.Y. Nam, D. Tham, J.E. Fischer, *Nano Lett.* 5 (2005) 2029.
- [12] R.M. Langford, T.X. Wang, D. Ozkaya, *Microelectron Eng.* 84 (2007) 784–788.
- [13] V. Gopal, E.A. Stach, V.R. Radmilovic, I.A. Mowat, *Appl. Phys. Lett.* 85 (2004) 49.
- [14] A.D. Franklin, Z. Chen, *Nat. Nanotechnol.* 5 (2010) 858–862.
- [15] D. Brunel, D. Deresmes, T. Mélin, The surface voltage drop across the set of electrodes is less than 3V, due to side-capacitance effects in KFM measurements, *Appl. Phys. Lett.* 94 (2009) 223508.
- [16] KFM experiments are not available for EBID contacted nanotubes due to low voltage drops along the device as a result of the EBID lead high resistance. c-AFM experiments would similarly provide local currents 4 to 6 orders of magnitude lower than for IBID electrodes (see Fig. 1), beyond detection limits.
- [17] R. Martel, T. Schmidt, H.R. Shea, T. Hertel, P. Avouris, *Appl. Phys. Lett.* 73 (1998) 2447.